Low potential manganese ions as efficient electron donors in native anoxygenic bacteria

Sasmit S. Deshmukh, Charles Protheroe, Matei-Alexandru Ivanescu, Sarah Lag, László Kálmán

PII: S0005-2728(18)30002-1
DOI: https://doi.org/10.1016/j.bbabio.2018.01.002
Reference: BBABIO 47861

To appear in:

Received date: 19 September 2017
Revised date: 20 December 2017
Accepted date: 16 January 2018

Please cite this article as: Sasmit S. Deshmukh, Charles Protheroe, Matei-Alexandru Ivanescu, Sarah Lag, László Kálmán , Low potential manganese ions as efficient electron donors in native anoxygenic bacteria. The address for the corresponding author was captured as affiliation for all authors. Please check if appropriate. Bbabio(2018), https://doi.org/10.1016/j.bbabio.2018.01.002

Low potential manganese ions as efficient electron donors in native anoxygenic bacteria

Sasmit S. Deshmukh[a], Charles Protheroe[a], Matei-Alexandru Ivanescu[a], Sarah Lag[a], and László Kálmán[a]*

[a]Department of Physics, Concordia University, Montreal, QC, Canada

*Corresponding author: Laszlo Kalman, 7141. Sherbrooke Street West, Montreal, QC, H4B 1R6, Canada; email: laszlo.kalman@concordia.ca

Abstract: Systematic control over molecular driving forces is essential for understanding the natural electron transfer processes as well as for improving the efficiency of the artificial mimics of energy converting enzymes. Oxygen producing photosynthesis uniquely employs manganese ions as rapid electron donors. Introducing this attribute to anoxygenic photosynthesis may identify evolutionary intermediates and provide insights to the energetics of biological water oxidation. This work presents effective environmental methods that substantially and simultaneously tune the redox potentials of manganese ions and the cofactors of a photosynthetic enzyme from native anoxygenic bacteria without the necessity of genetic modification or synthesis. A spontaneous coordination with bis-tris propane lowered the redox potential of the manganese (II) to manganese (III) transition to an unusually low value (~400 mV) at pH 9.4 and allowed its binding to the bacterial reaction center. Binding to a novel buried binding site elevated the redox potential of the primary electron donor, a dimer of bacteriochlorophylls, by up to 92 mV also at pH 9.4 and facilitated the electron transfer that is able to compete with the wasteful charge recombination. These events impaired the function of the natural electron donor and made BTP-coordinated manganese a viable model for an evolutionary alternative.

Keywords: photosynthesis, electron transfer, energy conversion, evolution, manganese

Abbreviations: Bacterial Reaction Center (BRC); Primary electron donor of bacterial photosynthesis (P); Primary electron donor of oxygenic photosynthesis (P_{680}), Oxygen Evolving Complex (OEC); terminal electron acceptor (Q_B); Wild type (WT), carotenoid-less strain (R-26); *Rhodobacter* (*Rba*); *N*-lauryl-*N*-*N*-dimethylamine-*N*-oxide (LDAO); Ethylenediaminetetraacetic acid (EDTA); 2,3-dimethoxy-5-methyl-6-polyprenyl-1,4-benzoquinone (ubiquinone, UQ); bis-tris propane (BTP); Bacteriochlorophyll (BChl), Bacteriopheophytin (BPheo).

1. Introduction

One of the critical milestones of the evolution of life on Earth is linked to the transition from anoxygenic to oxygen producing photosynthesis about 2.8-2.4 billion years ago [1- 4]. Models have been proposed to account for the numerous molecular requirements that had to be satisfied over the transition period [5, 6]. One of the key elements required for oxygen evolution is the ability to use manganese ions as rapid secondary electron donors [7]. Efficient utilization of manganese in the native bacterial reaction center (BRC) from purple anoxygenic photosynthetic bacteria has been considered energetically unfavorable (Fig. 1 left) as the primary electron donor (P) has lower potential (0.5 V) than that of the manganese sources readily available [5, 8].

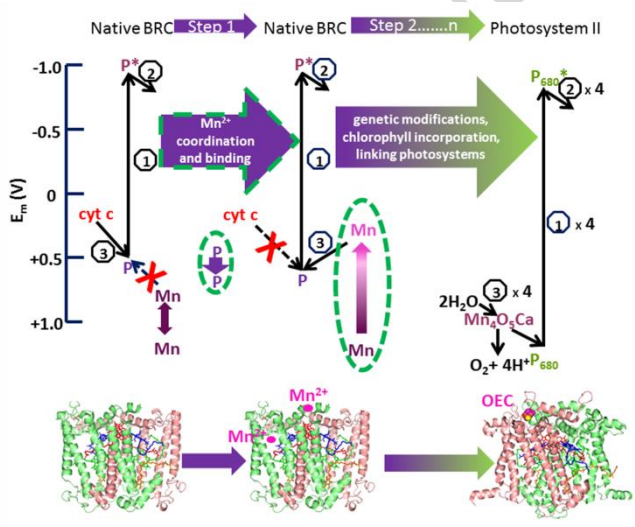

Fig. 1. Energetics of light-induced electron transfer steps at the donor side of photosystems. The redox potentials of the primary and secondary electron donors are indicated in the BRC (left), in Photosystem II (right), and in native BRC, where manganese oxidation is enabled by coordination and binding (middle). The electron transfer sequence is labeled by numbers in octagons for the electronic excitation of P or P_{680}, for the charge separation, and for the electron donation from the secondary electron donors, respectively. Only reactions marked by thin

downhill arrows are spontaneous. Vertical block arrows indicate tuning of redox potentials. To demonstrate the structural similarities, the L and M subunits of BRC (PDB: 1PCR) and the D1 and D2 proteins of Photosystem II (PDB: 3WU2) are shown in salmon and green colors, respectively. The location of the OEC (Mn_4O_5Ca) and the proposed binding of Mn^{2+} are also indicated.

Contrarily, the primary electron donor (P_{680}) in Photosystem II can deploy high potential electron donors (Fig. 1 right), including manganese ions from the oxygen evolving complex (OEC) [7]. Photosystem II and BRC are evolutionary related as plants and cyanobacteria share a common ancestor with purple photosynthetic bacteria [9]. Despite the differences in the energetics surrounding the primary and secondary donors, the structural details and the mechanism of the transmembrane electron transfer are analogous in these two enzymes [5, 8, 10, 11]. Generation of the proton gradient across the membrane, a key feature for the survival of the organism, requires subsequent electron transfer steps that lead to the double reduction and double protonation of the terminal electron acceptors (secondary quinones; Q_B) in both systems. This process is only possible if the oxidized primary electron donors, P^+ and P_{680}^+, are rapidly reduced by secondary electron donors in BRC and PSII, respectively. Electron transfer reactions from donors unique to oxygenic photosynthesis, such as light-driven tyrosine and manganese oxidation have been introduced to BRCs, however, thus far exclusively via multiple genetic modifications [12-14]. In these modified BRCs the redox potential of P was elevated by up to ~0.3 V by design and introduction of up to four mutations. Two-to-five mutations were necessary to observe manganese oxidation and at least five mutations were required to witness tyrosine oxidation. The electron transfer in these modified BRCs from the secondary electron donors to P^+ was effective

as it successfully competed with the charge recombination reactions. A slow photo-oxidation of manganese(II) ions in native BRCs was reported in the presence of bicarbonate (BCT), however, the electron transfer from Mn^{2+} to P^{+} there was found at least two orders of magnitude slower than the charge recombination and the yield was only ~5% [15]. Here we describe how spontaneous coordination of manganese with hydroxyl and amine groups and its binding to native BRCs can tune the redox potentials of both manganese and P substantially. The electron transfer between Mn^{2+} and P^{+} not only can compete with the charge recombination but also approaches 100% yield. As solely environmental factors were required to gain this attribute our system may serve as a proof of principle for the earliest step in the development of oxygenic photosynthesis (Fig. 1 middle) that does not require genetic modification.

2. Materials and Methods

2.1. Bacterial growth and BRC isolation.

Cells from wild type (WT) and the carotenoid-less R-26 strains of *Rhodobacter (Rba.) sphaeroides* were grown anaerobically under light. The RCs were isolated and purified using *N*-lauryl-*N*-*N*-dimethylamine-*N*-oxide (LDAO) according to methods described earlier [16,17]. Ethylenediaminetetraacetic acid (EDTA), a potent chelator, was removed from the samples by extensive dialysis. For some experiments the LDAO detergent was replaced with Triton X-100 (TX-100) by ion exchange chromatography. In some experiments 100 μM terbutryn was used to block the electron transfer between the quinones while in others the secondary quinone activity was reconstituted with either UQ_{10} or UQ_0 (2,3-dimethoxy-5-methyl-6-polyprenyl-1,4-benzoquinone).

2.2.Preparation of the manganese complex.

Manganous acetate or chloride was dispersed in 0.03 % LDAO containing 80 mM bis-tris propane (BTP) at pH 9.4. A 1 M stock was prepared and this stock was diluted to the desired final concentration. A fresh stock was used for each measurement. The manganese complex was added to BRCs that were previously pre-illuminated and allowed to recover from their corresponding charge-separated states. The measurements were performed after 30 minutes incubation time.

2.3. Optical spectroscopy

Optical spectra and some kinetics of the absorbance changes induced by continuous illumination or light pulse were measured using a Varian (Agilent) Cary 5000 spectrophotometer (Mulgrave, Victoria, Australia) according to methods described earlier [16-18]. The charge-separated states were induced either by continuous or pulsed illumination using high throughput fiber optics (Newport Corp., Irvine, CA, USA.). The continuous light source was either an Oriel 2129 tungsten lamp or an Oriel 6140 Arc lamp. The light intensity was varied between 0.13 and 1 W/cm^2. Laser flash-induced electron transfer reactions in the ms time scale were recorded with a miniaturized laser flash photolysis unit (LFP-112 from Luzchem Research Co., Ottawa, Ontario, Canada) as reported elsewhere [17]. Kinetic traces were analyzed by decomposition into exponentials using Marquardt-Levenberg nonlinear least-squares method.

2.4. Oxidation-reduction potential measurements

The oxidation-reduction midpoint potential of the P/P^+ and Mn^{2+}/Mn^{3+} couples were determined by spectroelectrochemical oxidation-reduction titrations as we described earlier [18]. The redox potential dependent light-induced absorption changes were determined using the same spectroelectrochemical redox cell. For these measurements the cell was tilted at $\sim 45^o$ angle with respect to the propagation of the monitoring beam and the actinic illumination was delivered

perpendicular to the window of the cell to avoid stray light entering the detector chamber [18]. At each selected potential value a short (~10 s) illumination was applied until the light-induced optical changes reached their equilibrium values. The absorption changes recorded at different potentials were fit with a single or a two component Nernst-equation.

2.5. Dual Polarization Interferometry (DPI)

Surface depositions of the BRCs and cytochrome were done using AnaLight Bio200 interferometer (Farfield Ltd., Manchester, U.K.) as described earlier [19,20]. The samples were delivered to the sensor chip (Unmodified AnaChip^{TM} FB 80, Farfield Ltd., Manchaster, U.K) by the integrated microfluidic system (Harvard Apparatus PHD 2000 pump) with a flow rate of 10 μL/min and was allowed to adsorb onto the surface of the chip. Once the sample delivery was finished (20 mins) the unbound samples above the chip were washed away by maintaining the flow of the running buffer revealing the tightly adsorbed layer. The camera response was analyzed in terms of layer thickness, density and deposited mass using Maxwell's equations [19].

2.6. Electron Paramagnetic Resonance (EPR) spectroscopy

Room temperature, X-band EPR spectra of the manganese complex and BRC were recorded with a MiniScope MS 5000 spectrometer (Freiberg Instruments, Freiberg, Germany). The spectra were recorded at 9.4 GHz frequency and 10 μW power. The field modulation was 0.2 mT (peak-to-peak) at 100 kHz. Single scans were recorded with 80 mT/minute scan rate. The photooxidation of manganese by BRC was performed in samples containing ~30 μM BRC, 0.03% LDAO, 300 mM manganous acetate, 80 mM BTP at pH 9.4. The spectra were recorded before and after a short illumination and the difference was computed representing the loss of Mn^{2+} due to oxidation by P^{+}.

2.7.Surface tension measurements

The surface tension of LDAO at different concentrations was determined by using DuNouy interfacial tensiometer (Central Scientific Co. Inc., Fairfax, VA, USA).

3. Results and discussion

3.1.Low Potential Manganese Mn-BTP complex .

The redox potential for the Mn^{2+}/Mn^{3+} transition in the aqueous hexa-aqua complex is over 1 V and exchanging some water ligands with bicarbonate anions still yields potential values higher than that of P found in native BRCs [13,21,22]. The lowest potential for Mn^{2+}/Mn^{3+} transition in proteins was reported for Mn-superoxide dismutase with a value of ~300 mV, where one of the ligands is a hydroxyl group besides the most frequent carboxylates and imidazoles [23-25]. To lower the potential of manganese we coordinated Mn^{2+} ions with bis-tris propane (BTP), a commonly used pH buffer, by simple mixing. The hydroxyl and secondary amine groups of BTP were reported to coordinate iron and manganese ions that form metal clusters but so far only via synthesis in biologically incompatible solvents [26]. Here the spontaneous coordination of Mn^{2+} with BTP was dependent upon the pH (see Supplementary Fig. S1) suggesting that the secondary amine groups were also involved as ligands in addition to the hydroxyl groups. The room temperature electron paramagnetic resonance (EPR) spectrum of the Mn-BTP complex at pH 8 was very similar to that of the mononuclear hexa-aqua complex signifying a similar mononuclear complex (see Supplementary Fig. S2A). Spectroelectrochemical redox titrations at pH 9.4 revealed a reversible transition involving one electron that was well characterized using a one component Nernst-equation with midpoint potential value of ~400 mV for the Mn^{2+}/Mn^{3+} couple (Fig. 2).

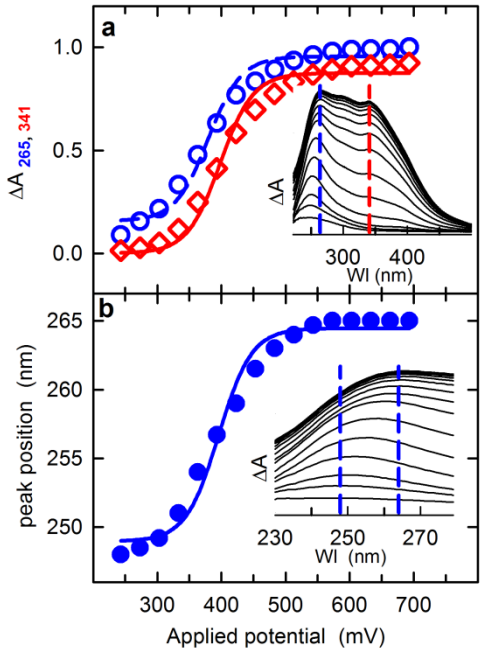

Fig. 2. Oxidation potential of Mn^{2+}/Mn^{3+} couple in the Mn-BTP complex. The difference optical spectra (inserts; actual potential-minus-base potential) were recorded in the range between 243 mV and 700 mV (vs. hydrogen electrode). The absorbance values at 265 nm (open blue circles), 341 nm (open red diamonds), and the band position (closed blue circles) were plotted against the applied potential. Single component Nernst equation was used to fit the data assuming the involvement of one electron. The fits yielded the following midpoint potential values for the Mn^{2+}/Mn^{3+} transition: 381 mV, 398 mV, and 396 mV obtained from absorbance values at 265 nm, 341 nm and from the band shift between 247 to 265 nm, respectively. The error of the fits is less than ± 6 mV. Conditions: 1 M manganous acetate in 0.05% TX-100, 80 mM BTP pH 9.4, 70 mM KCl.

3.2 Signatures of Mn^{2+} oxidation by P^+

The light-minus-dark optical difference spectrum of BRC at pH 9.4 showed notable differences depending on whether BTP-coordinated Mn^{2+} was present or absent (Fig. 3a). Without Mn^{2+} (black trace) the spectrum contained features of both P^+ and the semireduced quinone (Q^-) generally observed in the absence of secondary electron donors [12-14]. In the presence of Mn^{2+}, if coordinated with BTP (dark cyan trace), all signals characteristic to P^+ disappeared after a 5 s illumination demonstrating an electron donation from a potent electron donor, such as ferrocene (blue trace on Fig. 3a) [12-14]. Additionally, novel spectroscopic features, including a large (9 nm) electrochromic shift of the P-band from 865 nm to 856 nm and a band centered at 265 nm were identified after subtraction of the features characteristic to the semiquinones (grey trace). The former is a result of a strong charge–dipole interaction between Mn^{3+} and P and the latter was identified as characteristic of Mn^{3+} (see also Fig. 2 insert). Both theoretical calculations and experimental data showed that such large hypsochromic shifts of the P band are expected if positive charges are placed near rings C and E along the Q_y transition dipole of P [27,28]. The loss of Mn^{2+} in the EPR spectrum due to illumination of the BRC is also consistent with the photo-oxidation of Mn^{2+} to Mn^{3+} (Supplementary Fig. S2B). The rate of the electron transfer from Mn^{2+} to P^+ and the influence of Mn^{2+} on the charge recombination were probed by recording the kinetics of absorption changes at 865 nm, where P has a strong absorbance, both under saturating continuous illumination and after a single saturating light pulse excitation (Fig. 3b, c). Under strong continuous illumination the rate of manganese oxidation was 1.6-fold higher in the carotenoid-less strain (R-26) than in wild type (WT), with rate constants of 1.3 and 0.8 s^{-1}, respectively (Fig. 3b). These values are comparable with the rate constants of the charge recombination without Mn^{2+} (Fig. 2c) if the secondary quinone binding site is occupied [13,29].

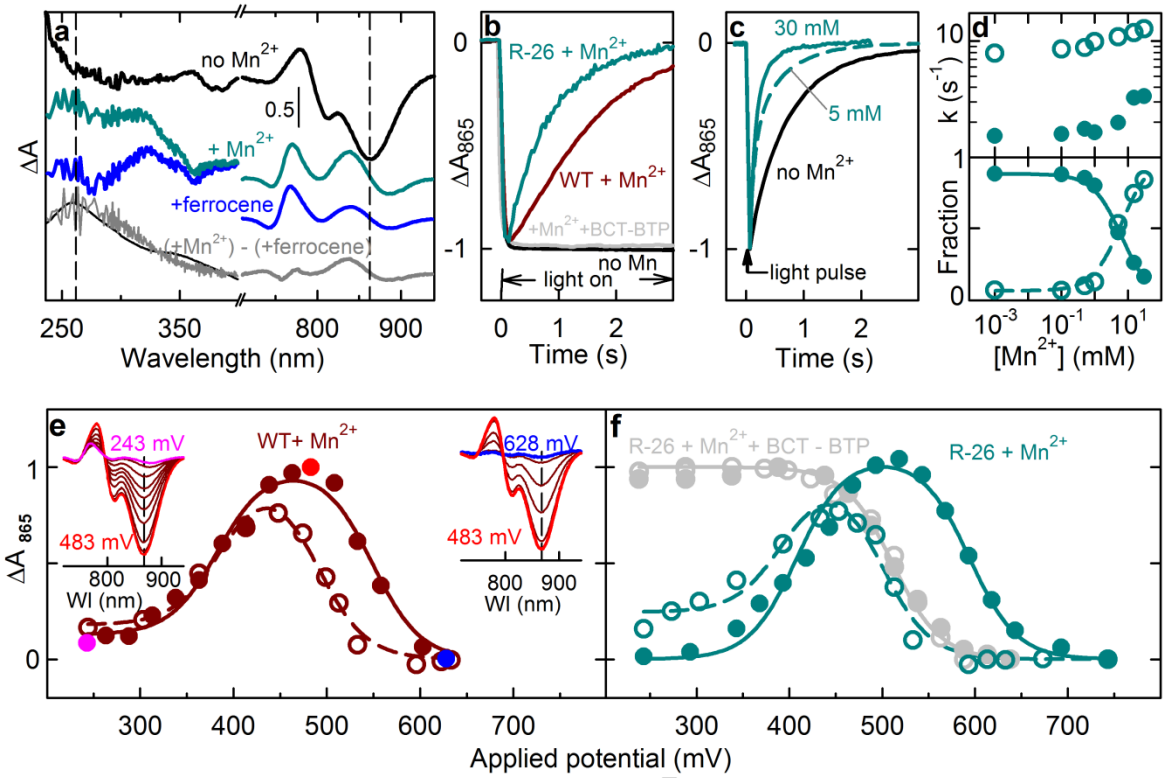

Fig. 3. Spectroscopic signatures of manganese oxidation at pH 9.4**.** (a) Light-minus-dark optical difference spectra of BRC. Vertical dashed lines at 865 nm and 265 nm indicate the band positions characteristic to P^+ and Mn^{3+}, respectively. The spectrum of the oxidized Mn-BTP complex (thin black trace) is also shown for comparison. (b) Kinetics of continuous light-induced manganese oxidation in BRCs from WT and R-26. (c) Representative kinetic traces of absorbance changes at 865 nm induced by a light pulse at different Mn^{2+} concentrations. (d) Rate constants (top) and relative amplitudes (bottom) of the fast (open circles) and slow (closed circles) kinetic components of the charge recombination as a function of Mn^{2+} concentration. Solid lines represent fits to binding equations with dissociation constants of 6.5 mM and 6.4 mM for the fast and slow components, respectively. (e, f) Light-induced absorption changes at 865 nm obtained at different applied potentials in WT and R-26 in the presence of manganese. Titrations were carried out both in the oxidative (closed circles) and reductive (open circles) directions. Lines represent fits to a two component Nernst-equation. The results for the fits are tabulated in Supplementary Table S1. Inserts show the light-induced spectra at different potentials in R-26 for oxidative direction.

Weaker illuminations resulted in slower observed kinetics in both strains that depended on the illumination intensity (Supplementary Fig. S3). Rapid manganese oxidation was only witnessed above pH 9 and the maximal rate was reached at 80 mM BTP concentration most likely due to the elevated potential of the Mn^{2+}/Mn^{3+} couple under suboptimal conditions (Supplementary Fig. S4A and S5). The steady state values of the P at different BTP concentration suggest that 2 BTP/Mn^{2+} are required for the rapid electron transfer (Supplementary Fig. S4B). The absorption at 865 nm in the same time scale did not change if BTP was replaced with BCT demonstrating that bicarbonate-coordinated manganous ions cannot donate an electron to P^+ efficiently (Fig. 3b, Supplementary Fig S9A). Addition of Mn^{2+} in the presence of BTP destabilized the $P^+Q_A^-$ and $P^+Q_B^-$ states (Fig. 3c) via charge-charge interactions as the rate constants for the charge recombination from these states (fast and slow components, respectively) increased with increasing Mn^{2+} concentration (Fig. 3d). Similar acceleration was reported earlier when positively charged residues were introduced or protons were trapped in the vicinity of P or P^+, respectively and resulted in elevated P/P^+ potentials [12-14,22, 30]. Manganese ions also appeared to trigger the displacement of Q_B, as the fraction of the slow component that accounts for the fraction of BRCs that have secondary quinone decreased with increasing Mn^{2+} concentration yielding an apparent dissociation constant of 6.5 mM (Fig. 3d). This observation suggests that Mn^{2+} ions must be able to access the Q_B binding site. Rapid electron transfer from Mn^{2+} to P^+ can be excluded as the optical spectrum after the single flash did not resemble that of the PQ^- state (Supplementary Fig. S5). The rapid (k = 13 s^{-1}) recovery kinetics of P^+ on Fig. 3c could only be assigned to electron donation from Mn^{2+} to P^+ if charge recombination between Mn^{3+} and Q_A^- would be feasible.

3.3 Binding of manganese to BRC elevates the potential of P

Spectroelectrochemical redox titrations of the BRCs in the presence of the Mn-BTP complex were performed, where the photo-induced charge separation and the subsequent electron transfer from Mn^{2+} to P^+ were probed by short illuminations while the redox potential was poised (Fig. 3e, f). The amount of P^+ detected at different applied potentials was governed by the *in situ* redox potentials of Mn^{2+}/Mn^{3+} and P/P^+ redox couples that allow different reactions to take place. At low potentials neither manganese nor P is oxidized by the applied potential so Mn^{2+} can reduce the photo-induced P^+ (pink spectrum in the insert of Fig. 3e). Intermediate potentials oxidize Mn^{2+} to Mn^{3+} , which is unable to reduce the photo-generated P^+ (red spectrum in panel e). High applied potentials create P^+ before the illumination and photo-oxidation of P to P^+ is no longer possible (blue spectrum in panel e). Hence, the dependence of the photo-oxidized dimer on the applied potential shows a bell shaped curve that can be characterized with the sum of two Nernst-curves: one characteristic to the Mn^{2+}/Mn^{3+} and the other to the P/P^+ transition (Fig. 3e,f). Significant variances were found in the redox potentials in R-26 and in WT indicating different degree of electrostatic repulsion between the charges on P^+ and on the Mn-cofactor (Supplementary Table S1). The Mn^{2+}/Mn^{3+} potential was raised in the presence of P^+ by 20 mV and the P/P^+ potential was elevated by 92 mV in the presence of manganese in R-26. Smaller shifts of the redox potentials in WT suggest weaker charge-charge interactions between the manganese and P^+. The redox potentials were sensitive to the direction of the titration resulting in a large hysteresis. Performing the titrations in the reductive direction restored the P/P^+ potential in both WT and R-26 to the value that can be obtained without Mn^{2+} (dashed lines in Fig. 3e, f). This observation is consistent with the Mn-cofactor being electrostatically repelled from its binding site if the positive charge on P^+ is retained for extended period of time. The electron donation from Mn^{2+} to P^+ and the hysteresis was completely absent and the P/P^+

potential was not elevated significantly if BTP was substituted by BCT (grey trace in Fig. 3f). The elevated P/P^+ potential in the presence of Mn-BTP from 500 mV to 592 mV at pH 9.4 in R-26 is consistent with the acceleration of the charge recombination between P^+ and Q_A^- from ~9 to ~13 s^{-1} (depicted earlier in Fig. 3c, d) and it suggests the presence of uncompensated charges near P. This is in good agreement with reports, where positively charged His residues were introduced at different positions near P, causing the P/P^+ potentials to be elevated to a range of 560 - 630 mV at pH 8 and a the corresponding charge recombination rates to increase from 10 s^{-1} to a range of 13 - 15 s^{-1}, respectively [13,22,30].

3.4. Identifying the manganese binding sites

Potential Mn^{2+} binding sites in the vicinity of P were explored by Q-SiteFinder, a binding site predictor server [31]. Two sites were identified that are within the range of effective biological electron transfer (Fig. 4, Supplementary Fig. S7, Video S1). One site is positioned at the periplasmic surface ~ 6 Å above P, where the native secondary electron donor, cytochrome (cyt) binds [32]. The second site was predicted at ~15 Å from the C and E rings of P_B in a hydrophobic cavity near the inactive bacteriochlorophyll monomer ($BChl_B$). The location of this site is near the position of the carotenoid molecule that marks the only difference between WT and R-26 and also provides access to all the B-side cofactors including the Q_B binding site. The place of the carotenoid can be empty or occupied by detergent molecules (e.g. LDAO) in R-26 [8]. Evidence of manganese binding was found at both predicted sites but proof of electron transfer could only be established from the hydrophobic site (Fig. 4).

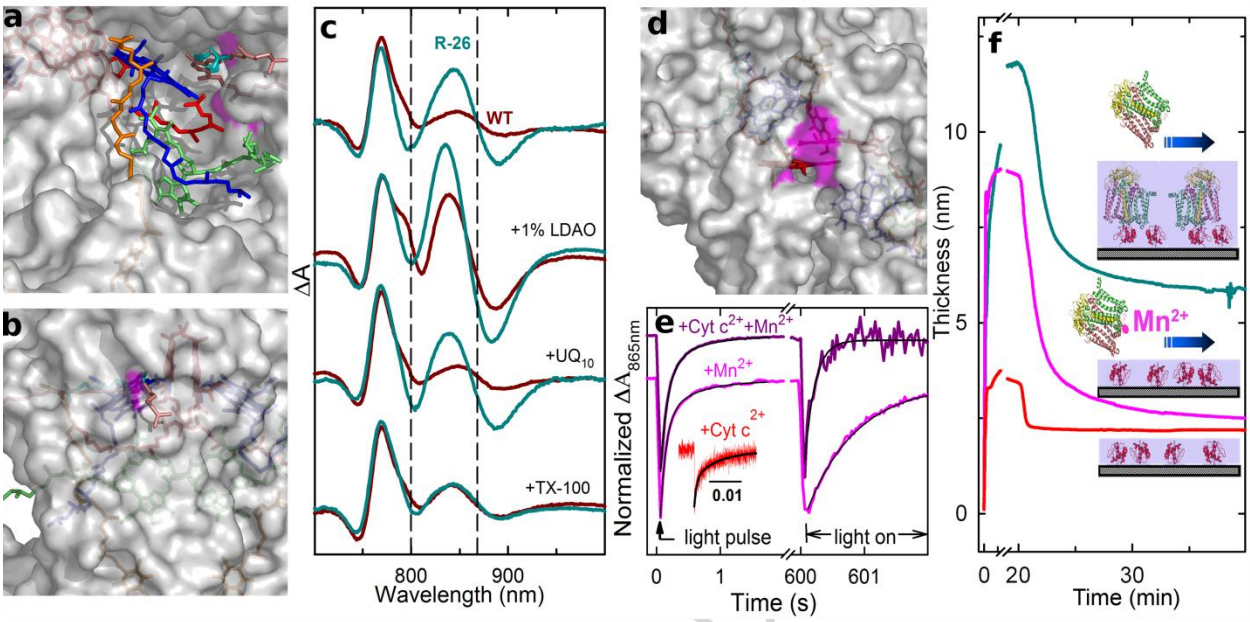

Fig. 4. Probing the proposed sites for binding and electron transfer**.** (a, b) Surface representations of the BRC featuring the hydrophobic cavity near $BChl_B$ and (d) the periplasmic surface: P, $BChl_B$, $Bpheo_B$, Q_B, carotenoid, and the zwitterionic LDAO are shown in red, blue, green, orange, salmon, and cyan, respectively. Residues in the proposed Mn^{2+} binding sites are displayed in magenta. The view from (a) to (b) was generated by ~80^o rotation to the left. PDB ID codes used: 1PCR, 1RG5. (c) Light-minus-dark optical difference spectra of BRC from WT and R-26 in the presence of Mn^{2+}. LDAO, UQ_{10}, and a nonionic detergent (TX-100) were applied to influence the electrochromic absorption changes around 800 and 865 nm (vertical dashed lines). (e) Kinetics of light-induced absorption changes at 865 nm in the presence of secondary donors: cyt (insert, red trace) Mn^{2+} (magenta), and cyt and Mn^{2+} together (purple). Black solid lines are the fits to exponentials. Results of the fits are listed in Supplementary Table S2. (f) Kinetic traces of single layer protein deposition for cyt only (red), premixed Mn^{2+}, cyt, and BRC (magenta), and premixed cyt and BRC (dark cyan), respectively.

The electrochromic absorption changes at ~865 nm and ~800 nm both in the dark and upon illumination suggest that manganese must be localized at the hydrophobic site along the direction of the Q_y transition dipoles of P and of $BChl_B$ (Fig. 4c, Supplementary Figs. S8-S10, Table S2, Video S1). Additionally, molecules (e.g. LDAO, ubiquinones, terbutryn) that are all known to have access and binding sites in the cavity had profound effects on these electrochromic absorption changes and on the kinetics of Mn^{2+} oxidation (Fig. 4c, Supplementary Figs. S9 – S12). Presence of excess LDAO decreased the rate of Mn^{2+} oxidation in R-26 to the level found in WT, as LDAO was able to bind to the carotenoid binding site but it had no effect on it in WT, where this site was already occupied (Supplementary Fig. S9). Contrarily, even very high concentrations of salt had small influence on the kinetics demonstrating limited solvent accessibility of the electron donating metal (Supplementary Fig. S11D, E). The influence of the partition coefficients on the apparent binding abilities of ubiquinones with different dielectric properties to the Q_B binding site has been demonstrated earlier [33]. Correspondingly, we found a 16-fold difference in the apparent inhibitor constants for manganese oxidation depending on whether the most hydrophobic (UQ_{10}) or the most hydrophilic (UQ_0) member was used from the ubiquinone family (Supplementary Fig. S11). Exact determination of the local concentration of free Mn^{2+} in the buried site is a challenge although other hydrophilic compounds, such as sodium borohydrate and glycerol were also reported to enter the hydrophobic cavities of BRCs [34,35]. Based on these arguments the apparent K_D of 6.5 mM (Fig. 3d) most likely significantly underestimates the true affinity of Mn^{2+} binding to the buried site.

3.5. *Manganese binding also impedes the natural electron donor*

The periplasmic site was probed by assessing cyt binding and oxidation in the presence of Mn^{2+} (Fig. 4e, f). The natural secondary electron donor, cyt c, can donate electrons in microseconds

under optimal conditions [36]. Above pH 9 this process was reported to slow down to milliseconds [37]. We found that presence of BTP alone did not alter this millisecond kinetics (Fig. 4e insert, Supplementary Table S2). However, when Mn^{2+} was also present at pH 9.4, the electron transfer rate from cyt to P^+ dramatically decreased and became comparable to that of the charge recombination and of the Mn-oxidation by P^+ (Fig. 4e, Supplementary Table S3). Single molecular layer deposition using dual polarization interferometry confirmed the displacement of cyt by Mn^{2+} at the periplasmic surface (Fig. 4f). Binding of BRC to cyt was only possible if Mn^{2+} was absent and the deposited average layer thickness in that case was consistent with the molecular size of the BRC-cyt complex. In the presence of Mn^{2+} a thinner layer was immobilized to the surface indicating cyt deposition only as the Mn-BRC complex was washed away due to lack of access to the cyt-binding site. We have found no evidence of electron transfer from the periplasmic Mn^{2+} as the observed Mn^{2+} oxidation kinetics could be influenced by molecules that are hydrophobic but not by screening surface charges (Supplementary Fig. S11D). The ultimate test for a viable secondary electron donor is whether it can support the formation of a proton gradient, which is required for the survival of the organism. In our system quinol formation was observed in the presence of excess native quinone (UQ_{10}) when manganese served as the sole secondary electron donor (Supplementary Fig. S12). The quinol formation is also supported by the 2 Mn^{2+}/UQ_{10} stoichiometry as the double reduction of Q_B requires two electrons to be transferred from the secondary donor to P^+ (Supplementary Fig. S11E). The 1 Mn^{2+}/UQ_0 stoichiometry is also consistent with the lack of binding of UQ_0 at high pH [33]. Despite the lack of strong binding of UQ_0 the excess quinoines in the cavity dilute the manganese locally and weaken the metal binding resulting in a slower electron donation from Mn^{2+} to P^+ (Supplementary Fig S11 A,B)

3.6. *Evolutionary implications*

Growing geological evidence suggests that manganese oxidizing photosynthesis must have existed prior to the rise of oxygen evolving cyanobacteria [38,39]. It is unclear whether the introduction of this attribute required genetic modifications to elevate the potential of the bacteriochlorophylls above that of the manganese or environmental conditions could have tuned the corresponding redox potentials without the necessity of genetic modifications [5,15,21,41]. This work provides a proof of concept for the latter scenario. The concentration range required for manganese oxidation here is consistent with the elevated levels of Mn^{2+} reported for the Archean seawater [21,40]. It is unlikely that BTP itself was available in the environment of photosynthetic bacteria at the time of the transition period as opposed to bicarbonate in the CO_2-rich atmosphere [15,21]. Bicarbonate-coordinated manganese, however, cannot serve as a viable electron donor as the wasteful charge recombination reactions are at least two orders of magnitude faster than the electron donation from manganese and its potential is still higher than that of P [13,15,22] (Fig. 3, Supplementary Fig. S9). BTP could be considered, however, as a model ligand for manganese coordination that presents a manganese cofactor that i) has an unusually low potential (Fig. 2), ii) can bind to native anoxygenic BRCs and donate electrons to P^+ efficiently (Fig. 3), iii) can support the generation of a proton gradient (Supplementary Fig. S12), and, iv) can inhibit the function of the native secondary electron donor (Fig. 4e). These attributes are all vital for an evolutionarily relevant electron donor that must have replaced the native cytochromes. Naturally abundant molecules with hydroxyl and amino groups (e.g. mixtures and adducts of amino acids) are currently being evaluated for manganese coordination and photo-oxidation.

Acknowledgements

This work was supported by grants from Natural Sciences and Engineering Research Council of Canada and from Canada Foundation for Innovation. We thank Professors James P. Allen and Péter Maróti for their suggestions.

References

1. Des Marais, D.J. When did photosynthesis emerge on earth? *Science* **289**, 1703-1705 (2000).
2. Brasier, M. D., Green, O. R., Jephcoat, A. P., Kleppe, A.P., Van Cranendonk, M. J., Lindsay, J. F., Steele, A. & Grassineau, N. V. Questioning the evidence for Earth's oldest fossils. *Nature* **416**, 76-81 (2002).
3. Rashby, S. E., Sessions, A. L., Summons, R.A. & Newman, D. K. Biosynthesis of 2-methylbacteriohopanepolyols by an anoxygenic phototroph. *Proc. Natl. Acad. Sci. U.S.A.* **104**,1 5099-15104 (2007).
4. Buick, R. When did oxygenic photosynthesis evolve? *Phyl. Trans. R. Soc. B* **363**, 2731-2743 (2008).
5. Blankenship, R. E.& Hartman. H. The origin and evolution of oxygenic photosynthesis. *Trends. Biol. Sci.* **23**, 94-97 (1998).
6. Larkum, A. W. D. The evolution of chlorophylls and photosynthesis, in *Chlorophylls and bacteriochlorophylls: biochemistry, biophysics, functions and applications*. Grimm,B. , Porra, R. J., Rüdiger, W. & Scheer, H. Eds. pp. 261-282, (Springer, 2006).

7. Yano, J. & Yachandra, V. Mn4Ca cluster in photosynthesis: Where and how water is oxidized to dioxygen. *Chem. Rev.* **114**, 4175-4205 (2014).

8. Hunter, N., Daldal, F., Thurnauer, M. & Beatty, J. T., Eds *The Purple Phototrophic Bacteria* (Springer-Verlag, 2009).

9. Xiong, J., Fischet, W. M., Inoue, K., Nakahara, M. & Bauer, C. E. Molecular evidence for the early evolution of photosynthesis. *Science* **289**, 1724-1730 (2000).

10. Ermler, U., Fritzsch, G., Buchanan, S.K.& Michel, H. Structure of the photosynthetic reaction centre from *Rhodobacter sphaeroides* at 2.65 Å resolution: cofactors and protein-cofactor interactions. *Structure* **2**, 925-936 (1994).

11. Umena, Y., Kawakami, K., Shen, J-R. & Kamiya, N. Crystal structure of oxygen-evolving photosystem II at a resolution of 1.9 Å. *Nature* **473,** 55-60 (2011).

12. Kálmán, L., LoBrutto, R., Allen, J. P. & Williams, J. C. Modified reaction centers oxidize tyrosines in reactions that mirror Photosystem II. *Nature* **402**, 696-699 (1999).

13. Kálmán, L., LoBrutto, R., Allen, J. P. & Williams J. C. Manganese oxidation by modified reaction centers from *Rhodobacter sphaeroides*. *Biochemistry* **42**, 11016-11022 (2003).

14. Thielges, M., Uyeda, G., Cámara-Artigas, A., Kálmán, L., Williams, J. C. & Allen, J. P. Design of a redox-linked active metal site: Manganese bound to the bacterial reaction center at a site resembling that of Photosystem II. *Biochemistry* **44**, 7389-7394 (2005).

15. Khorobrykh, A., DasGupta, J., Kolling, D. R. J., Terentyev, V., Klimov, V. V. & Dismukes, G. C. Evolutionary origins of the photosynthetic water oxidation cluster: Bicarbonate permits Mn^{2+} photooxidation by anoxygenic bacterial reaction centers. *Chem. Biochem.* **14**, 1725-1731 (2013).

16. Deshmukh, S. S., Tang, K. & Kálmán, L. Lipid binding to the carotenoid binding site in photosynthetic reaction centers. *J. Am. Chem. Soc.* **133**, 16309-16316 (2011).

17. Tang, K., Williams, J. C., Allen, J. P. & Kálmán, L. Effect of anions on binding and oxidation of divalent manganese and iron in modified bacterial reaction centers. *Biophys. J.* **98**, 3295-3304 (2009).

18. Deshmukh, S. S., Williams, J. C., Allen, J. P. & Kálmán, L. Light-Induced conformational changes in photosynthetic reaction centers: Redox regulated proton pathway near the dimer. *Biochemistry* **50,** 3321-3331 (2011).

19. Balhara, V., Deshmukh, S. S., Kálmán, L. & Kornblatt, J. A. The interaction of Streptococcal Enolase with Canine Plasminogen: The role of surfaces in complex formation *Plos One* **9**, e88395 (2014).

20. Escorihuela, J., González-Martínez, M. Á., López-Paz, J. L., Puchades, R., Maquieira, Á. & Gimenez-Romero, D. Dual-Polarization Interferometry: A novel technique to light up the nanomolecular world. *Chem. Rev.* **115**, 265-294 (2015)

21. Dismukes, C. G., Klimov, V. V., Baranov, S.V., Kozlov, Y. N., DasGupta, J. & Tyryshkin, A. The origin of atmospheric oxygen on Earth: The innovation of oxygenic photosynthesis. *Proc. Natl. Acad. Sci. U.S.A.* **98**, 2170-2175 (2001).

22. Kálmán, L., Wiliams, J.C. & Allen, J. P. Energetics for oxidation of a bound manganese cofactor in modified bacterial reaction centers. *Biochemistry* **50,** 3310-3320 (2011).

23. Miller, A-F. Superoxide dismutases: ancient enzymes and new insights. *FEBS Lett.* **58**6, 585-595 (2012).

24. Christianson, D. W. Structural chemistry and biology of manganese metalloenzymes. *Prog. Biophys. Mol. Biol.* **67**, 217–252 (1997).

25. Edwards, R. A., Baker, H. M., Whittaker, M. M., Whittaker, J. W., Jameson, J. B. & Baker, E. M. Crystal structure of Escherichia coli superoxide dismutase in 2.1 Å resolution. *J. Biol. Inorg. Chem.* **3**, 161-171 (1998).

26. Ferguson, A., Darwish, A., Graham, K., Schmidtmann, M., Parkin, A. & Murrie, M. Bis-tris propane as a new polydentate linker in the synthesis of iron (III) and manganese (II/III) Complexes. *Inorg. Chem.* **47**, 9742-9744 (2008).

27. Hanson, L. K., Thompson, M. A., Zerner, M. C. & Fajer, J. in *The Photosynthetic Bacterial Reaction Center I*, Breton, J.& Vermeglio, A., Eds, pp 355-367 (Plenum Press, New York, 1989).

28. Kálmán, L., LoBrutto, R., Narvaez, A. J., Williams. J. C. & Allen, J. P. Correlation of proton release and electrochromic shifts of the optical spectrum due to oxidation of tyrosine in reaction centers from *Rhodobacter sphaeroides*. *Biochemistry* **42**, 13280-13286 (2003).

29. Paddock, M. L., Feher, G. & Okamura, M.Y. Proton and electron transfer to secondary quinone (Q_B) in bacterial reaction centers: The effect of changing the electrostatics in the vicinity of Q_B by interchanging Asp and Glu at the L212 and L213 sites. *Biochemistry* **36**, 14238-14249 (1997).

30. Lin, X., Murchison, H. A., Nagarajan, V., Parson, W. W., Allen, J. P. & Williams, J. C. Specific alteration of the oxidation potential of the electron donor in reaction centers from *Rhodobacter sphaeroides. Proc. Nat. Acad. Sci. U.S.A.* **91**, 10265-10269 (1994).

31. Laurie, A. T.R. & Jackson, R. M. Q-SiteFinder: An energy based method for the prediction of protein-ligand binding sites. *Bioinformatics* **21**,1908-1916 (2005).

32. Axelrod, H. L. Abresch, H. L., Okamura, M. Y., Yeh, A. P., Rees, D. C. & Feher, G. X-ray structure determination of the cytochrome c(2): Reaction center electron transfer complex from *Rhodobacter sphaeroides*. *J. Mol. Biol.* **319**, 501-515 (2002).

33. McComb, J. C., Stein, R. R. & Wraight, C. A. Investigations on the influence of headgroup substitution and isoprene side-chain length in the function of primary and secondary quinones of bacterial reaction centers. *Biochim. Biophys. Acta* **1015**, 155-161 (1990).

34. Koepke, J., Krammer, E-M., Klingen, A. R., Sebban, P., Ullmann, G. M. & Fritzsch, G. pH modulates the quinone position in the photosynthetic reaction center from *Rhodobacter sphaeroides* in the neutral and charge separated states. *J. Mol. Biol.* **371**, 396-409 (2007).

35. Maróti, P., Kirmaier, C., Wraight, C. A., Holten, D. & Pearlstein, R. M. Photochemistry and electron transfer in borohydrate-treated photosynthetic reaction centers. *Biochim. Biophys. Acta* **810**, 132-139 (1985).

36. Venturoli, G., Drepper, F., Williams, J. C., Allen, J.P., Lin, X. & Mathis, P. Effects of temperature and ΔG^o on electron transfer from cytochrome c(2) to the photosynthetic reaction center of the purple bacterium *Rhodobacter sphaeroides*. *Biophys. J.* **74**, 3226-3240 (1995).

37. Osváth, S. & Maróti, P Coupling of cytochrome and quinone turnovers in the photocycle of reaction centers from the photosynthetic bacterium *Rhodobacter sphaeroides*. *Biophys. J.* **73**, 972-982 (1997).

38. Johnson, J. E., Webb, S. M., Thomas, K., Ono, S., Kirschvink, J. L. & Fischer, W. W., Manganese-oxidizing photosynthesis before the rise of cyanobacteria. *Proc. Natl. Acad. Sci. U.S.A.* **108**, 11238-11243 (2013).

39. Allen, J. F. & Martin, W. Evolutionary biology: Out of thin air. *Nature* **445,** 610-612 (2007).

40. Fischer, W. W. & Knoll, A. H. An iron shuttle for deep water silica in Late Archean and early Paleoproterozoic iron formation. *Geol. Soc. Am. Bull.* **121**, 222-235 (2009).

41. Hohmann-Marriott, M.F. & Blankenship, R. E. Evolution of Photosynthesis. *Annu. Rev. Plant. Biol.* **52**, 515-546 (2011).

Low potential manganese ions as efficient electron donors in native anoxygenic bacteria

Sasmit S. Deshmukh[a], Charles Protheroe[a], Matei-Alexandru Ivanescu[a], Sarah Lag[a], and László Kálmán[a]*

Highlights

- Mn^{2+}/Mn^{3+} redox potential is lowered to ~400 mV without the need of synthesis
- Electron transfer from Mn^{2+} to P^{+} in native anoxygenic reaction centers is efficient
- Mn^{2+} binds to two sites in native reaction centers if coordinated by bis-tris propane
- Mn^{2+} binding elevates the P/P^{+} potential by up to ~100 mV
- Mn^{2+} binding impedes the natural electron donor, cytochrome
- Mn^{2+} can support quinol formation in native reaction centers